NMR Surface Relaxivity in a Time-Dependent Porous System

Neil Robinson, Razyq Nasharuddin, Einar O. Fridjonsson, and Michael L. Johns*
Department of Chemical Engineering, The University of Western Australia, 35 Stirling Highway, Perth, Western Australia 6009, Australia

(Received 14 October 2022; accepted 21 February 2023; published 23 March 2023)

We demonstrate an unexpected decay-recovery behavior in the time-dependent ^{1}H NMR relaxation times of water confined within a hydrating porous material. Our observations are rationalized by considering the combined effects of decreasing material pore size and evolving interfacial chemistry, which facilitate a transition between surface-limited and diffusion-limited relaxation regimes. Such behavior necessitates the realization of temporally evolving surface relaxivity, highlighting potential caveats in the classical interpretation of NMR relaxation data obtained from complex porous systems.

DOI: 10.1103/PhysRevLett.130.126204

While functional porous materials underpin a vast array of processes of importance to the energy, environment, chemical, and construction sectors, characterization of key structural and interfacial properties within such systems is severely hampered by their optically opaque nature. Nuclear magnetic resonance (NMR) relaxation measurements (also termed nuclear spin relaxation measurements) provide a versatile and nondestructive approach with which to probe the dynamics of spin-bearing fluids within porous materials [1,2], and have been applied widely to the study of both equilibrium fluid properties (informing pore size distributions [3,4], adsorption phenomena [5,6] and diffusive exchange processes [7,8]) and to obtain time-resolved insight into evolving material structures (such as cements [9–13]). In this Letter we expand upon the established interpretation of NMR relaxation data when probing such time-resolved material properties, elucidating the uniquely coupled sensitivity of such measurements to the temporal evolution of both pore structure characteristics and surface chemistry properties simultaneously.

For fluid-saturated porous media, expressions for the dependence of observed ^{1}H (proton) longitudinal (T_1) and transverse (T_2) NMR relaxation behavior on pore structure and interfacial chemistry are well known, taking the general form [14]

$$\frac{1}{T_i} \approx \frac{1}{T_{i,\mathrm{bulk}}} + \left(\frac{d}{2\alpha\rho_i} + \frac{d^2}{8\alpha D}\right)^{-1}, \tag{1}$$

wherein $i \in \{1, 2\}$, and where additional terms may be required to fully account for observed T_2 relaxation rates in the presence of magnetic susceptibly contrast across the solid-fluid interface [15,16]; such effects are mitigated in this work by performing our measurements at low magnetic field [17]. Here, T_i are the observed (measured) time constants and $T_{i,\mathrm{bulk}}$ represent the time constants for the unrestricted bulk fluid. Terms within parentheses then describe the extent to which pore structure and interfacial chemistry perturb the observed relaxation characteristics: d is the pore diameter, α is a dimensionless shape parameter (taking values of 1, 2, or 3 for planar, slit, or cylindrical pores, respectively), and D is the self-diffusion coefficient of the confined fluid. The terms ρ_i are the (spatially averaged) surface relaxivities of the solid-fluid interface, which may be modeled as $\rho_i = \lambda/T_{i,\mathrm{surf}}$ [18], where $T_{i,\mathrm{surf}}$ are the relaxation time constants within an adsorbed surface layer of thickness λ. Such terms describe enhanced rates of relaxation which occur at solid-fluid interfaces both due to a reduction in molecular mobility within the adsorbed surface layer [19] and through dipolar proton-electron interactions between adsorbate-bound ^{1}H and paramagnetic species on the pore surface [14]. Established limiting cases for such relaxation dynamics exist. In the limit $D/d \ll \rho_i$ for instance, surface relaxation rates are significantly more rapid than the rates of diffusive transport across the pores, with Eq. (1) reducing to

$$\frac{1}{T_i} \approx \frac{1}{T_{i,\mathrm{bulk}}} + \frac{8\alpha D}{d^2}. \tag{2}$$

Conversely, in the limit $D/d \gg \rho_i$, diffusion across the pore is sufficiently more rapid than the rates of enhanced surface relaxation at the pore surface, with Eq. (1) reducing to

$$\frac{1}{T_i} \approx \frac{1}{T_{i,\mathrm{bulk}}} + \frac{2\alpha\rho_i}{d}. \tag{3}$$

Such limits are referred to according to the overall rate controlling process; Eq. (2) therefore describes diffusion-limited relaxation, while Eq. (3) describes surface-limited relaxation. Here, we discuss data which for the first time permit clear identification of a temporal transition between

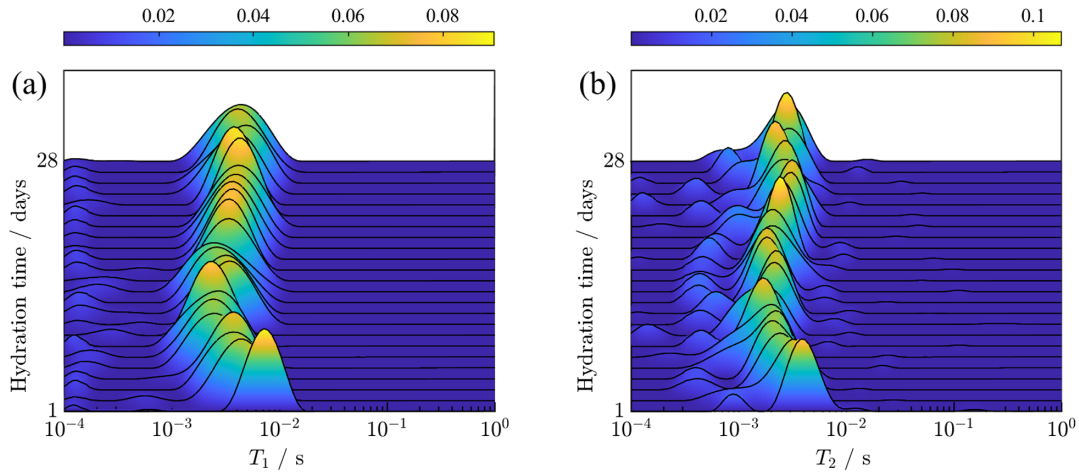

FIG. 1. Example (a) T_1 and (b) T_2 relaxation distributions for the hydrating material investigated in this study. Relaxation data were acquired over the first 28 days of material hydration. Color bars define the probability density of each relaxation distribution.

these limiting regimes within an evolving three-dimensional porous microstructure.

Figure 1 shows ^{1}H T_1 and T_2 distributions obtained at low magnetic field ($B_0 = 0.05$ T; $\nu_0(^1\mathrm{H}) = 2$ MHz) for tap water within the hydrating engineering material cemented paste backfill (CPB) [20–22]. This porous material comprised a mixture of spherical fly ash particles, minerals tailings, ordinary Portland cement, and water (see Supplemental Material [23] for extended details of materials preparation), with the solids containing 7.9 wt%, 3.2 wt %, and 2.6 wt% Fe_2O_3, respectively, as measured by inductively coupled plasma optical emission spectroscopy, wherein paramagnetic Fe^{3+} ions provide the dominant source of relaxation sinks for adsorbed water at the pore surface. NMR measurements were performed under ambient conditions using inversion recovery [29] and CPMG (Carr-Purcell Meiboom-Gill) NMR pulse sequences [30,31], respectively, with the resulting data inverted to produce probability density distributions of observed T_1 and T_2 times via Tikhonov regularization [32–34] (see Supplemental Material [23] for extended NMR methods). Acquired T_1 distributions [Fig. 1(a)] show a large primary peak, typical of systems in which sufficiently slow T_1 relaxation characteristics allow extensive diffusive mixing between water confined within different pore sizes [35]. Acquired T_2 distributions [Fig. 2(a)], which are naturally more sensitive to local pore geometry than T_1 due to shorter relaxation times, reveal multiple relaxation environments, indicative of water confined within a hierarchically porous cement structure. Such distributions are consistent with established models of cement hydration [36], with the assignment of these relaxation peaks to specific hydrating pore structures detailed elsewhere [37,38].

In this Letter we consider only the modal relaxation times from each inverted distribution, termed $\langle T_1 \rangle$ and $\langle T_2 \rangle$, respectively, which are dominated by the most populous pore structures within the hydrating material under study (capillary pores in traditional cement chemistry notation [39]). In recent work investigating the hydration behavior of a similar material in the absence of fly ash particles, a clear monoexponential relationship was observed between these modal time constants and hydration time t_h, which defines the experimental period across which the material is allowed to evolve. This relationship took the form $\langle T_i \rangle_{\mathrm{sl}} = a_i \exp(-b_i t_h) + c_i$ [37], where b_i are the observed material hydration rates, a_i provides a scaling factor, and c_i are offset parameters necessary to account for nonzero pore sizes at long t_h; the subscript "sl" indicates that surface-limited relaxation is assumed within this system [38]. Fitting $\langle T_i \rangle_{\mathrm{sl}}$ against t_h then enables the extraction and comparison of material hydration rates b_i, facilitating quantitative contrast between different material formulations, preparation procedures, and hydration conditions.

Figures 2(a) and 2(b) detail the temporal evolution of our acquired $\langle T_1 \rangle$ and $\langle T_2 \rangle$ data across 28 days of hydration. Rather than the expected monoexponential decay behavior, however, a clear decay-recovery process (subscript "dr") is observed for each data set which may be modeled as

$$\langle T_i \rangle_{\mathrm{dr}} = a_i' \exp(-b_i' t_h) - a_i \exp(-b_i t_h) + c_i. \quad (4)$$

We rationalize this biexponential behavior through consideration of a transition between the diffusion- and surface-limited relaxation processes described in Eqs. (2) and (3). In our chosen material the use of fly ash introduces a high Fe_2O_3 content (7.9 wt% as measured by inductively coupled plasma optical emission spectroscopy), providing a significantly increased paramagnetic Fe^{3+} concentration ($[Fe^{3+}]$) compared to that present in previous relaxation investigations of similar hydrating materials [37,38]. Surface relaxivity values $\rho_i = \lambda / T_{i,\mathrm{surf}}$ are sensitive to $[Fe^{3+}]$ via the established expressions [10,14]

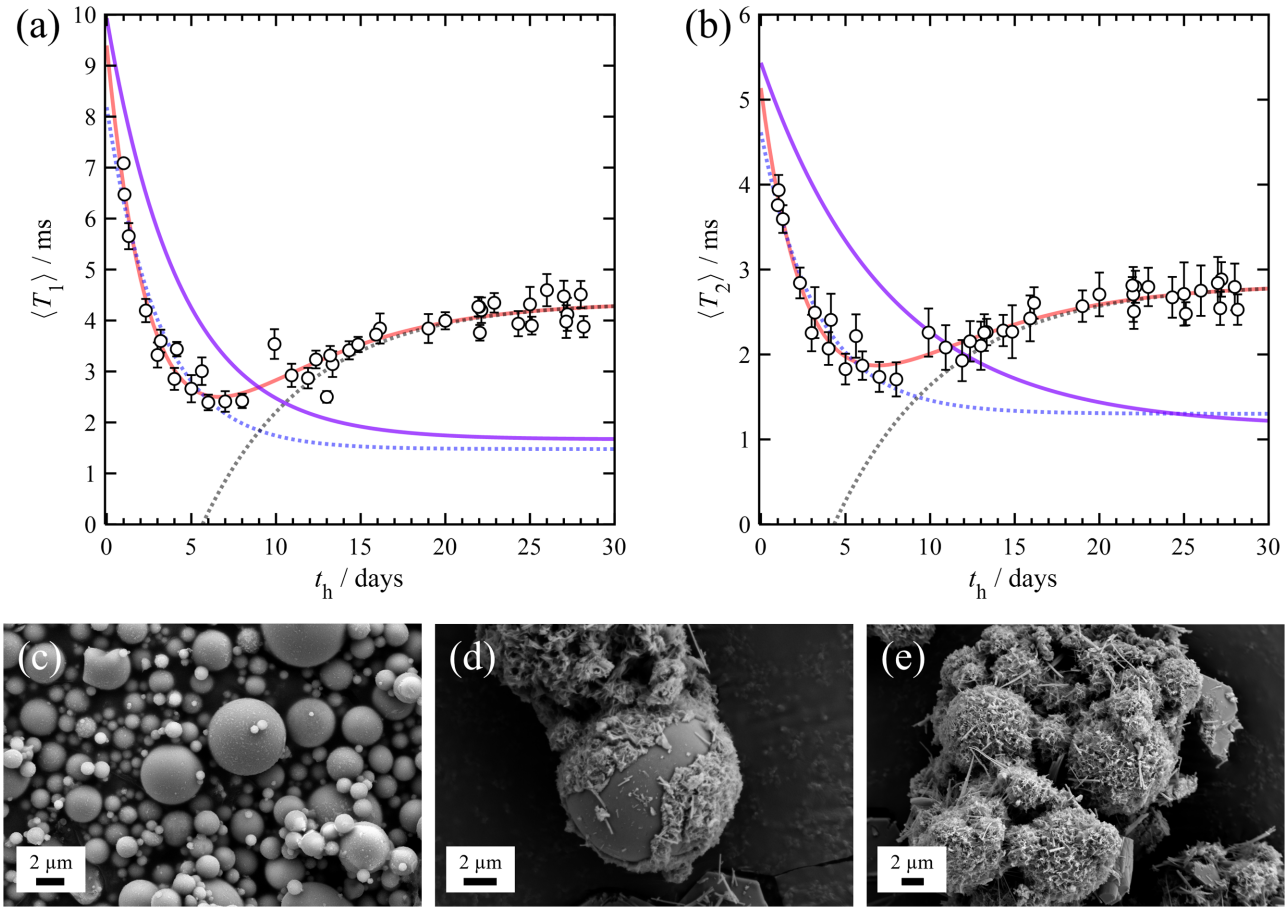

FIG. 2. (a) $\langle T_1 \rangle$ and (b) $\langle T_2 \rangle$ ^{1}H NMR relaxation evolution of water confined within the hydrating CPB material investigated here over 28 days. Error bars indicate ± 1 standard deviation ($n = 3$), while data points without error bars were acquired only once. Red curves indicate a fit to Eq. (4) with $b_i' = 2b_i$. Blue curves show monoexponential fits to data at $t_h < 10$ d, while gray curves represent the deconvoluted recovery components of Eq. (4), respectively. Purple curves show fitted monoexponential decay data obtained from similar hydrating systems in the absence of highly paramagnetic fly ash [37], demonstrating reduced decay rates relative to our data at short t_h. Bottom panels illustrate SEM images of fly ash particles; (c) shows fly ash particles in the absence of any cement hydration products ($t_h = 0$); while (d) and (e) evidence surface C-S-H adlayer formation following 7 and 14 days of hydration, respectively.

$$\frac{1}{T_{1,\mathrm{surf}}} = \beta\,[3J(\omega_I) + 7(\omega_S)],$$
$$\frac{1}{T_{2,\mathrm{surf}}} = \frac{\beta}{2}[8J(0) + 3J(\omega_I) + 13(\omega_S)], \qquad (5)$$

where the spectral density functions $J(\omega_x) = \tau_m \ln[1 + \omega_x^2\tau_m^2/(\tau_m^2/\tau_s^2) + \omega_x^2\tau_m^2]$ (with $x \in \{I, S\}$) capture the relationship between surface ^{1}H relaxation rates and the dynamics of adsorbed water molecules at the internal pore surfaces of the hydrating material [14]. Here, the correlation times τ_m and τ_s are the translational correlation time of water molecules between paramagnetic relaxation sinks, and the surface residence time before desorption, respectively, while the frequencies ω_I and ω_S are obtained via $\omega_x = \gamma_x B_0$, where γ_I and γ_S are the proton and electron gyromagnetic ratios, respectively [40]. Importantly, the prefactor is given by $\beta \propto \sigma\delta^{-4}\gamma_I^2\gamma_S^2\hbar^2 S(S+1)$, where σ is the density of paramagnetic surface species of spin S at the pore surface (and hence assumed directly dependent on $[Fe^{3+}]$ for our system; $S = 5/2$ for Fe^{3+}); δ is the distance of closest approach between adsorbate molecule and surface spins, while $\hbar$ is the reduced Plank constant [10].

Godefroy *et al.* demonstrated a dependence between $[Fe^{3+}]$ and limiting relaxation regime for a series of model porous structures comprising silicon carbide grains [14,41], evidencing a clear transition between diffusion-limited and surface-limited relaxation upon material cleaning to reduce $[Fe^{3+}]$. In the present work we conjecture that the temporal evolution of our hydrating porous material serves to facilitate this transition. Specifically, the dissolution-precipitation reactions responsible for cement hydration processes lead to the deposition of calcium silicate hydrate (C-S-H in cement chemistry notation) adlayers at the material pore surface [42], which is expected to both decrease the capillary pore size and limit access to the

highly paramagnetic fly ash particles upon increasing hydration time. We support this interpretation in Fig. 2 via scanning electron microscope (SEM) imaging of a sample of our hydrating material, which clearly demonstrates the time-dependent deposition of C-S-H across fly ash particle surfaces during the hydration period investigated. At short t_h we therefore interpret our observed relaxation behavior as dominated by interactions with high $[Fe^{3+}]$ fly ash particles [Fig. 2(c)]; following Eq. (5) these interactions facilitate large ρ_i values, causing pore water to undergo diffusion-limited ^{1}H relaxation (subscript "dl") according to Eq. (2). A result of the above interpretation is that a square dependence on pore size is expected during pore structure evolution at short t_h, of the form $T_i \propto d^2$. Given the established monoexponential decay relationship between $\langle T_i \rangle_{\mathrm{sl}}$ and t_h in the absence of fly ash cobinder [of the form $\langle T_i \rangle_{\mathrm{sl}} \sim d \sim \exp(-b_i t_h)$ [37]], an initial decay of the form $\langle T_i \rangle_{\mathrm{dl}} \sim d^2 \sim \exp(-2b_i t_h)$ is then expected from our present data; this rapid decay processes is accounted for by the primed components of our biexponential model expression in Eq. (4). As a simple visual comparison, blue dotted decay curves within Figs. 2(a) and 2(b) show a scaled monoexponential fit to our $\langle T_1 \rangle$ and $\langle T_2 \rangle$ data at $t_h < 10$ d [with decay rates constrained to equal those obtained from our full fit to Eq. (4) described below], while fitted relaxation data obtained from a comparable hydrating material in the absence of highly paramagnetic fly ash are shown in purple (data obtained from Ref. [37]; further details are provided in Supplemental Material [23]). Enhanced relaxation time decay rates are clearly evident in the presence of fly ash (blue dotted curves), providing support for the expectation of comparably large ρ_i values, and hence for the interpretation of diffusion-limited relaxation at short t_h. Note that given these two hydrating materials are likely characterized by different pore structures and surface relaxivities, quantitative comparisons between the relaxation time values exhibited by these two systems are not possible, and we make no attempt to ascribe a physical interpretation to the convergence of these curves at short t_h, which can only be coincidental.

Following nucleation at the solid-liquid interface, C-S-H deposits continue to grow across the available pore surfaces according to established mechanisms of cementitious hydration [36]. The evolution of such adlayers is demonstrated for the present system in Figs. 2(d) and 2(e), which reveal the difference in adlayer growth following $t_h = 7$ d and $t_h = 14$ d, respectively. As C-S-H adlayers cover the internal surfaces of the hydrating pore network, dipolar interactions between the high concentration of fly ash-bound Fe^{3+} and ^{1}H spins associated with confined pore water will be reduced, decreasing the spatially averaged surface relaxivity ρ_i of the capillary pore structures; such continued adlayer growth is therefore fundamental in initiating the proposed transition between diffusion- and surface-limited relaxation. An associated transition time may be estimated and will be associated with the shortest measured $\langle T_1 \rangle$ and $\langle T_2 \rangle$ times, which in the present work occur at $t_h \approx 7$ d. While the continuous temporal growth and deposition of surface adlayers serves to reduce the material pore sizes over time, this process continues to be convoluted with the above reduction in ρ_i. Such pore size changes do not lead to a continuous reduction in $\langle T_i \rangle_{\mathrm{dr}}$ as would occur within systems exhibiting classical surface-limited relaxation wherein ρ_i values are assumed time independent ($d\rho_i/dt_h \approx 0$). Rather, we interpret the observed *increase* in $\langle T_i \rangle_{\mathrm{dr}}$ with increasing t_h as a direct consequence of the coupling between pore structure evolution and decreasing ρ_i; this $\langle T_i \rangle$ recovery process is deconvoluted in gray within Figs. 2(a) and 2(b) and is accounted for by the second exponential term of Eq. (4).

A consequence of the above discussion is that we may now directly interpret b_i within Eq. (4) as material hydration rates, which are equated with the rate of changing surface relaxivity under surface-limited conditions. Appropriate fitting of our data to this expression with the constraint $b_i' = 2b_i$ was performed [red curves in Figs. 2(a) and 2(b)], yielding hydration rates $b_1 = 0.16 \pm 0.02\ \mathrm{d}^{-1}$ and $b_2 = 0.15 \pm 0.02\ \mathrm{d}^{-1}$. Remarkably, these values are in excellent agreement with previously observed CPB hydration rates of 0.08–0.2 d^{-1} obtained in the absence of fly ash [37]. This result provides both confidence in the above data interpretation and suggests that the assumption of $d\rho_i/dt_h \approx 0$ in the absence of fly ash is reasonable. We note for completeness that while $b_1 \approx b_2$ here, such equivalence is not necessarily expected given the differing sensitivities of $\langle T_1 \rangle$ and $\langle T_2 \rangle$ to the fine structure of hierarchical pore networks within hydrating cementlike materials (demonstrated in Fig. 1).

In summary, this work has demonstrated the measurement of nuclear spin relaxation phenomena within a dynamic and temporally evolving three-dimensional porous structure exhibiting changes to both pore size and pore surface chemistry. Our observations provide clear evidence that the ^{1}H NMR relaxation characteristics of water confined within such systems can exhibit sensitivity to both phenomena simultaneously, and that our measured relaxation data are susceptible to the resulting temporal changes in pore structure surface relaxivity. We anticipate the consideration of such time dependent surface relaxation phenomena will be critical in avoiding the erroneous interpretation of time-resolved relaxation data obtain from complex porous materials, especially when considering systems containing potentially high concentrations of paramagnetic species, or in reactive (catalytic) systems, where, e.g., the coking of polar pore surfaces is expected through the formation of reaction byproducts.

The authors thank Professor Andy Fourie (The University of Western Australia) for providing materials. R. N. acknowledges support from an Australian

Government Research Training Scholarship and N. R. acknowledges support from the Forrest Research Foundation. The authors further acknowledge use of the Australian Microscopy & Microanalysis Research Facility at The University of Western Australia Centre for Microscopy, Characterisation and Analysis.

*Corresponding author.
michael.johns@uwa.edu.au

[1] J.-P. Korb, Multiscale nuclear magnetic relaxation dispersion of complex liquids in bulk and confinement, Prog. Nucl. Magn. Reson. Spectrosc. **104**, 12 (2018).

[2] Y. Q. Song, Magnetic resonance of porous media (MRPM): A perspective, J. Magn. Reson. **229**, 12 (2013).

[3] S. Davies and K. J. Packer, Pore-size distributions from nuclear magnetic resonance spin-lattice relaxation measurements of fluid-saturated porous solids. I. Theory and simulation, J. Appl. Phys. **67**, 3163 (1990).

[4] S. Davies, M. Z. Kalam, K. J. Packer, and F. O. Zelaya, Pore-size distributions from nuclear magnetic resonance spin-lattice relaxation measurements of fluid-saturated porous solids. II. Applications to reservoir core samples, J. Appl. Phys. **67**, 3171 (1990).

[5] N. Robinson, E. F. May, and M. L. Johns, Low-field functional group resolved nuclear spin relaxation in mesoporous silica, ACS Appl. Mater. Interfaces **13**, 54476 (2021).

[6] J. Marreiros, R. de Oliveira-Silva, P. Iacomi, P. L. Llewellyn, R. Ameloot, and D. Sakellariou, Benchtop *in situ* measurement of full adsorption isotherms by NMR, J. Am. Chem. Soc. **143**, 8249 (2021).

[7] K. E. Washburn and P. T. Callaghan, Tracking Pore to Pore Exchange Using Relaxation Exchange Spectroscopy, Phys. Rev. Lett. **97**, 175502 (2006).

[8] N. H. Williamson, A. M. Dower, S. L. Codd, A. L. Broadbent, D. Gross, and J. D. Seymour, Glass Dynamics and Domain Size in a Solvent-Polymer Weak Gel Measured by Multidimensional Magnetic Resonance Relaxometry and Diffusometry, Phys. Rev. Lett. **122**, 068001 (2019).

[9] F. Barberon, J. P. Korb, D. Petit, V. Morin, and E. Bermejo, Probing the Surface Area of a Cement-Based Material by Nuclear Magnetic Relaxation Dispersion, Phys. Rev. Lett. **90**, 116103 (2003).

[10] P. J. McDonald, J.-P. Korb, J. Mitchell, and L. Monteilhet, Surface relaxation and chemical exchange in hydrating cement pastes: A two-dimensional NMR relaxation study, Phys. Rev. E **72**, 011409 (2005).

[11] D. Snoeck, L. Pel, and N. de Belie, Comparison of different techniques to study the nanostructure and the microstructure of cementitious materials with and without superabsorbent polymers, Constr. Build. Mater. **223**, 244 (2019).

[12] K. Friedemann, F. Stallmach, and J. Kärger, NMR diffusion and relaxation studies during cement hydration—A non-destructive approach for clarification of the mechanism of internal post curing of cementitious materials, Cement and Concrete Research **36**, 817 (2006).

[13] A. C. A. Muller, K. L. Scrivener, A. M. Gajewicz, and P. J. McDonald, Densification of C-S-H measured by 1H NMR relaxometry, J. Phys. Chem. C **117**, 403 (2013).

[14] S. Godefroy, J.-P. Korb, M. Fleury, and R. G. Bryant, Surface nuclear magnetic relaxation and dynamics of water and oil in macroporous media, Phys. Rev. E **64**, 021605 (2001).

[15] J. Mitchell and T. C. Chandrasekera, Understanding generalized inversions of nuclear magnetic resonance transverse relaxation time in porous media, J. Chem. Phys. **141**, 224201 (2014).

[16] P. R. J. Connolly, W. Yan, D. Zhang, M. Mahmoud, M. Verrall, M. Lebedev, S. Iglauer, P. J. Metaxas, E. F. May, and M. L. Johns, Simulation and experimental measurements of internal magnetic field gradients and NMR transverse relaxation times (T2) in sandstone rocks, J. Pet. Sci. Eng. **175**, 985 (2019).

[17] J. Mitchell, T. C. Chandrasekera, M. L. Johns, L. F. Gladden, and E. J. Fordham, Nuclear magnetic resonance relaxation and diffusion in the presence of internal gradients: The effect of magnetic field strength, Phys. Rev. E **81**, 026101 (2010).

[18] Y. Q. Song, H. Cho, T. Hopper, A. E. Pomerantz, and P. Z. Sun, Magnetic resonance in porous media: Recent progress, J. Chem. Phys. **128**, 052212 (2008).

[19] N. Robinson, C. Robertson, L. F. Gladden, S. J. Jenkins, and C. D'Agostino, Direct correlation between adsorption energetics and nuclear spin relaxation in a liquid-saturated catalyst material, ChemPhysChem **19**, 2472 (2018).

[20] C. Qi and A. Fourie, Cemented paste backfill for mineral tailings management: Review and future perspectives, Miner. Eng. **144**, 106025 (2019).

[21] R. Nasharuddin, G. Luo, N. Robinson, A. Fourie, M. L. Johns, and E. O. Fridjonsson, Cemented paste backfill compressive strength enhancement via systematic water chemistry optimisation, Constr. Build. Mater. **347**, 128499 (2022).

[22] E. Sadrossadat, H. Basarir, G. Luo, A. Karrech, R. Durham, A. Fourie, and M. Elchalakani, Multi-objective mixture design of cemented paste backfill using particle swarm optimisation algorithm, Miner. Eng. **153**, 106385 (2020).

[23] See Supplemental Material at http://link.aps.org/supplemental/10.1103/PhysRevLett.130.126204 for supplementary materials, methods and results, which includes Refs. [24–28].

[24] J. Keeler, *Understanding NMR Spectroscopy* (Wiley, New York, 2010).

[25] J. D. Wilson, Statistical approach to the solution of first-kind integral equations arising in the study of materials and their properties, J. Mater. Sci. **27**, 3911 (1992).

[26] E. O. Fridjonsson, A. Hasan, A. B. Fourie, and M. L. Johns, Pore structure in a gold mine cemented paste backfill, Miner. Eng. **53**, 144 (2013).

[27] K. Yang, E. S. Pouya, L. Liu, M. Li, X. Yang, N. Robinson, E. F. May, and M. L. Johns, Low-field NMR relaxation analysis of high-pressure ethane adsorption in mesoporous silicas, ChemPhysChem **23**, e202100794 (2022).

[28] K. G. Hollingsworth and M. L. Johns, Measurement of emulsion droplet sizes using PFG NMR and regularization methods, J. Colloid Interface Sci. **258**, 383 (2003).

[29] R. L. Vold, J. S. Waugh, M. P. Klein, and D. E. Phelps, Measurement of spin relaxation in complex systems, J. Chem. Phys. **48**, 3831 (1968).

[30] H. Y. Carr and E. M. Purcell, Effects of diffusion on free precession in nuclear magnetic resonance experiments, Phys. Rev. **94**, 630 (1954).

[31] S. Meiboom and D. Gill, Modified spin-echo method for measuring nuclear relaxation times, Rev. Sci. Instrum. **29**, 688 (1958).

[32] A. N. Tikhonov and V. I. A. Arsenin, *Solutions of Ill-Posed Problems* (SIAM, Philadelphia, 1977).

[33] G. H. Golub, M. Heath, and G. Wahba, Generalized cross-validation as a method for choosing a good ridge parameter, Technometrics **21**, 215 (1979).

[34] J. D. Griffith, A. E. Bayly, and M. L. Johns, Evolving microstructures in drying detergent pastes quantified using NMR, J. Colloid Interface Sci. **315**, 223 (2007).

[35] P. T. Callaghan, *Translational Dynamics and Magnetic Resonance: Principles of Pulsed Gradient Spin Echo NMR* (Oxford University Press, New York, 2011).

[36] J. W. Bullard, H. M. Jennings, R. A. Livingston, A. Nonat, G. W. Scherer, J. S. Schweitzer, K. L. Scrivener, and J. J. Thomas, Mechanisms of cement hydration, Cement and Concrete Research **41**, 1208 (2011).

[37] R. Nasharuddin, G. Luo, N. Robinson, A. Fourie, M. L. Johns, and E. O. Fridjonsson, Understanding the microstructural evolution of hypersaline cemented paste backfill with low-field NMR relaxation, Cement and Concrete Research **147**, 106516 (2021).

[38] N. Robinson, R. Nasharuddin, G. Luo, A. Fourie, E. O. Fridjonsson, and M. L. Johns, Pore structure evolution of cemented paste backfill observed with two-dimensional NMR relaxation correlation measurements, Ind. Eng. Chem. Res. **60**, 13253 (2021).

[39] M. Wyrzykowski, A. M. Gajewicz-Jaromin, P. J. McDonald, D. J. Dunstan, K. L. Scrivener, and P. Lura, Water redistribution–microdiffusion in cement paste under mechanical loading evidenced by ^{1}H NMR, J. Phys. Chem. C **123**, 16153 (2019).

[40] S. Godefroy, M. Fleury, F. Deflandre, and J.-P. Korb, Temperature effect on NMR surface relaxation in rocks for well logging applications, J. Phys. Chem. B **106**, 11183 (2002).

[41] J. P. Korb, S. Godefroy, and M. Fleury, Surface nuclear magnetic relaxation and dynamics of water and oil in granular packings and rocks, Magn. Reson. Imaging **21**, 193 (2003).

[42] H. M. Jennings, Refinements to colloid model of C-S-H in cement: CM-II, Cement and Concrete Research **38**, 275 (2008).